Treatment planning adaptation in ion beam therapy using sparse in-room ion radiographies

Markus Schöttle, Ines Butz, Julian Titze, Hector Andrade Loarca, Ozan Öktem, Gitta Kutyniok, Katia Parodi, Chiara Gianoli

Chair of Experimental Physics – Medical Physics
Faculty for Physics
Ludwig-Maximilians-Universität München

Ion Imaging Workshop 2025 - Florence, Italy - 20-21 October 2025

The role of ion imaging in ion beam therapy

- In current clinical practice, ion beam therapy still relies on X-ray imaging
- X-ray imaging introduces inaccuracies in the patient model due to semi-empirical calibration from linear attenuation to relative stopping power
- Ion imaging provides direct relative stopping power information, potentially eliminating or reducing these inaccuracies in treatment planning
- As an in-room modality, ion imaging offers also potential for adaptive radiation therapy

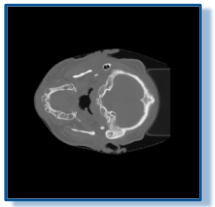

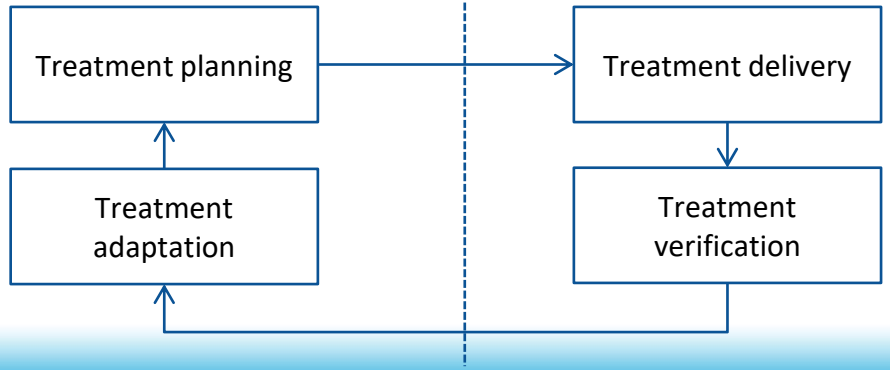

The role of ion imaging in ion beam therapy

- The investigation of the role of ion imaging in treatment planning targets the calibration inaccuracies

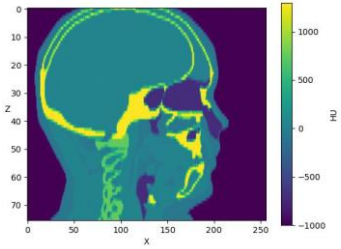

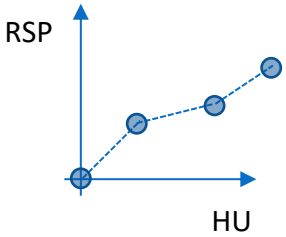

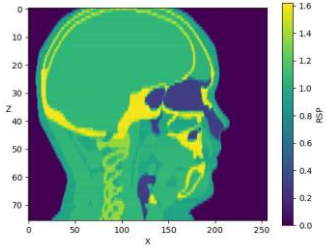

Rationale of the work of Ines Butz

- The investigation of the role of ion imaging in treatment adaptation targets inter-fractional anatomical changes occurring between treatment planning and treatment delivery due to physiological deformations

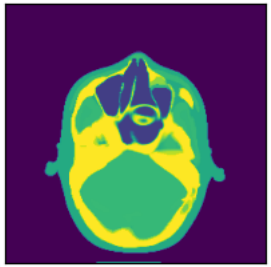

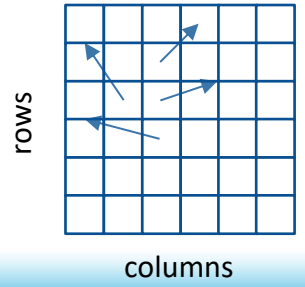

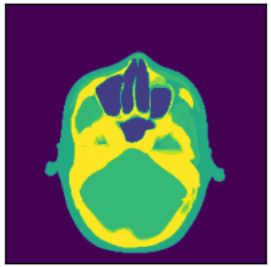

The role of ion imaging in ion beam therapy

- Both problems have been proposed and investigated using conventional methodologies (i.e., model-based approaches) within the framework of the project “Hybrid ImaGing framework in Hadrontherapy for Adaptive Radiation Therapy” (HIGH ART), financed by the *Deutsche Forschungsgemeinschaft* (DFG)
  - A pathway for clinical translation from X-ray to ion imaging is envisioned through the combination of X-ray and ion imaging based on sparse ion radiographies, for both treatment planning and treatment adaptation
- Within the framework of the renewal project, the reinterpretation of both problems in terms of machine learning and deep learning (i.e., data-driven approaches) has been proposed and investigated

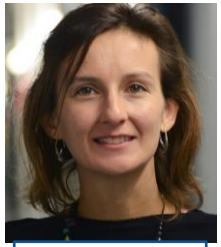
Chiara Gianoli


Katia Parodi


Prasannakumar Palaniappan


Ines Butz

Gefördert durch
DFG Deutsche Forschungsgemeinschaft

The Learned Primal-Dual network

- The Learned Primal-Dual (LPD) network, originally developed for deep image reconstruction, is investigated to solve the registration problem based on sparse ion radiographies

  - The LPD network is composed by 10 Primal-Dual blocks

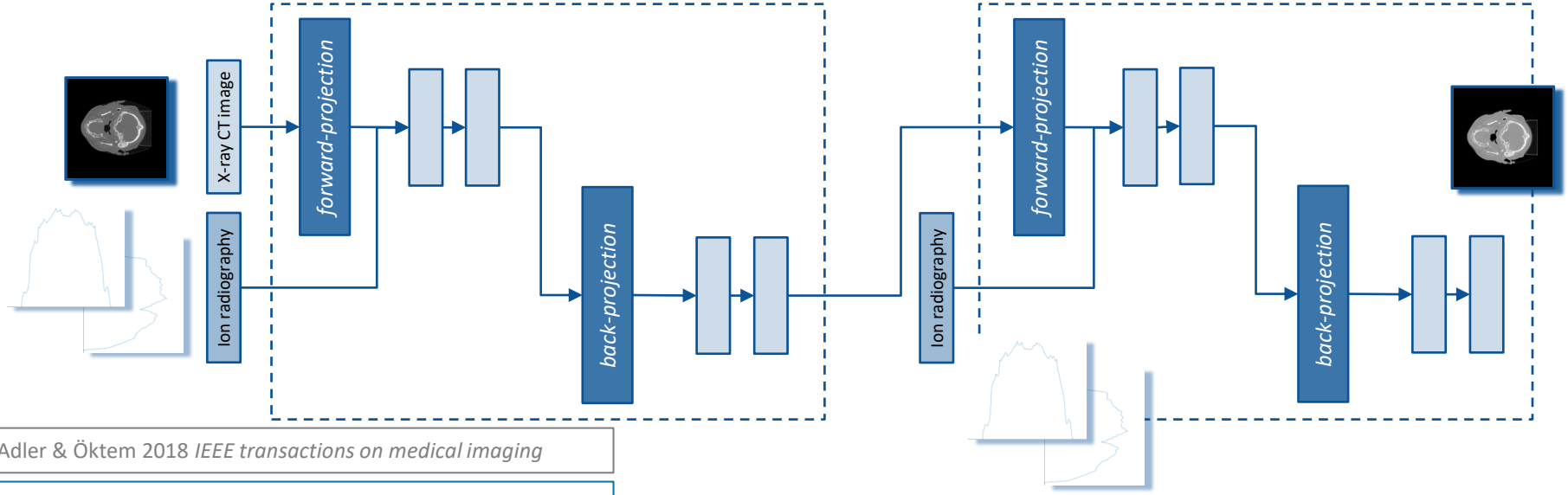

Adler & Öktem 2018 *IEEE transactions on medical imaging*

Butz, …, Parodi, Gianoli 2025 *Phys. Med. Biol. (under revision)*

The extended Learned Primal-Dual network

- An extension of the Learned Primal-Dual network based on a U-Net architecture is proposed, referred to as U-LPD network

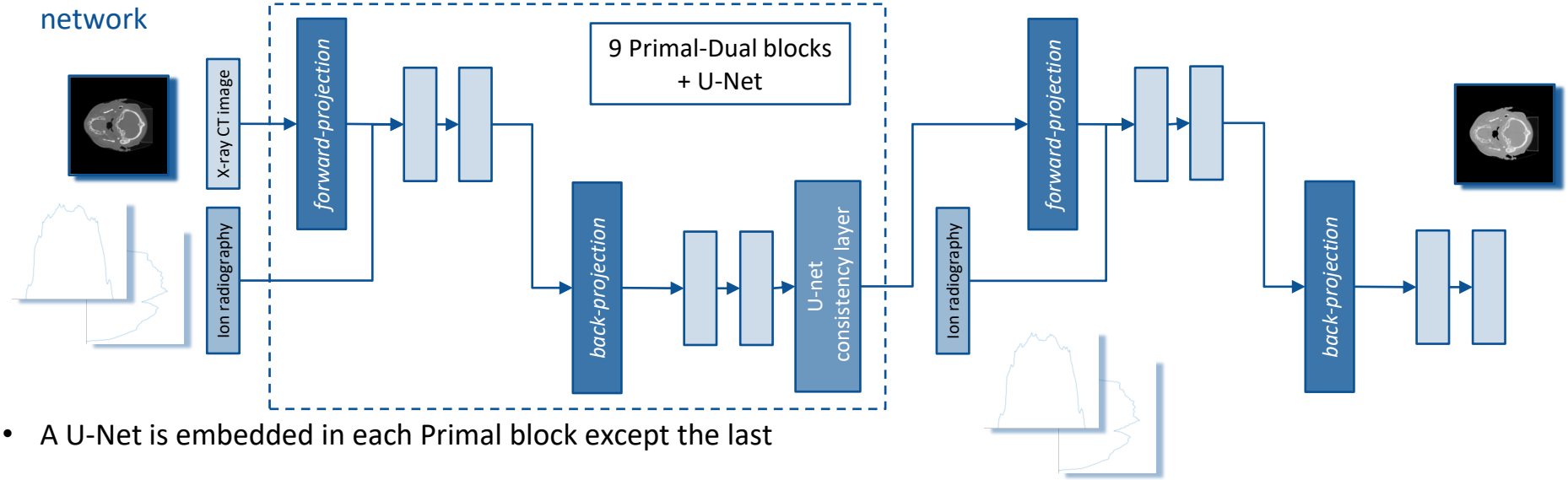

- A U-Net is embedded in each Primal block except the last
- To enforce consistency between the U-Net output and the radiographies, a consistency layer is incorporated

$$Primal_{consistent} = Primal_{U-net} + BP(Dual - FP(Primal_{U-net}))$$

U-net embedded in the Learned Primal-Dual network

- Base filter = 4
- Channel expansion factor = 2 (4 → 8 → 16)
- Number of layers = 3

- 3D convolution (3×3×3) + ReLU
- Concatenative skip connection
- Max pooling
- 3D transposed convolution (3×3×3)

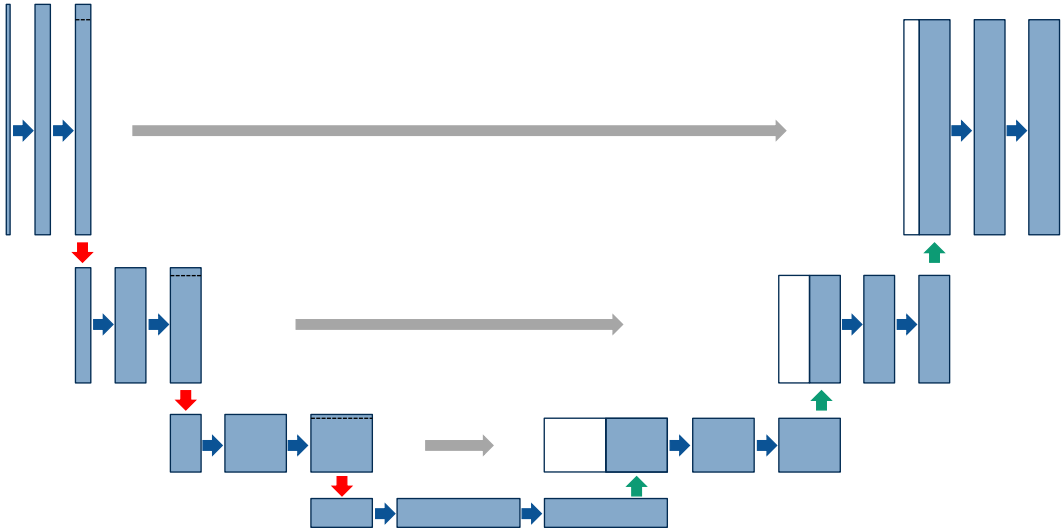

Definition of sparse ion radiographies

- The dataset is composed by ten original anthropomorphic phantoms, calibrated from linear attenuation to relative stopping power, assumed as ground truth images
  - Each slice is calibrated according to a randomly generated calibration curve
- Ion radiographs are generated by forward-projecting the ground truth images, simulating the in-room treatment delivery scenario
  - A total of five radiographies are considered, uniformly distributed over 180 degrees

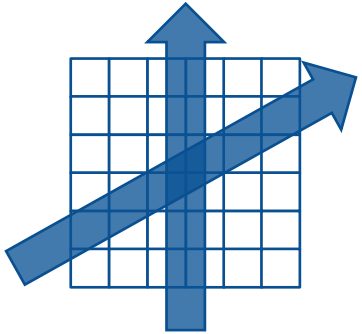

0 degree | 36 degrees | 72 degrees | 108 degrees | 144 degrees

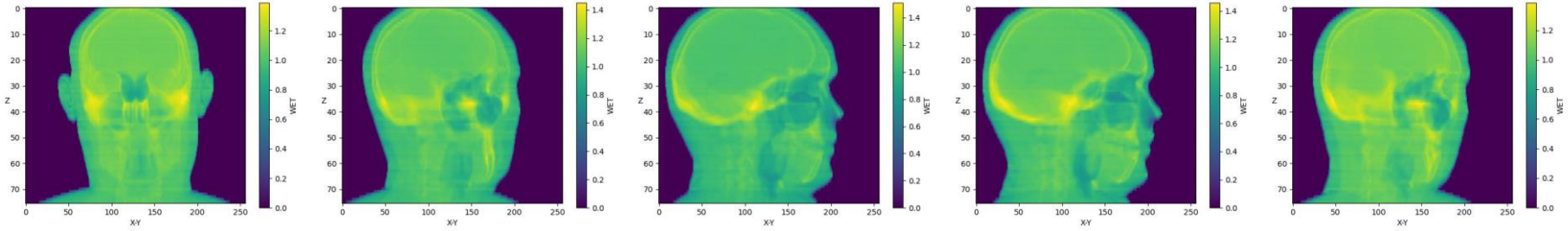

Definition of transformation fields

- To generate the treatment planning scenario, controlled anatomical changes are applied to the ground truth images by deforming the phantoms using Gaussian derivative-based transformations, simulating effects such as tissue shrinkage and dilation

- The deformation field is defined based on anisotropic Gaussian derivative functions

$$G(x,y,z) = \exp\left(- \left[\frac{(x - \mu_x)^2}{2\,\sigma_x^2} + \frac{(y - \mu_y)^2}{2\,\sigma_y^2} + \frac{(z - \mu_z)^2}{2\,\sigma_z^2} \right] \right)$$

$$G_x = -\alpha_x \left(\frac{(x - \mu_x)}{\sigma_x^2} \right) G \quad G_y = -\alpha_y \left(\frac{(y - \mu_y)}{\sigma_y^2} \right) G$$

$$G_z = -\alpha_z \left(\frac{(z - \mu_z)}{\sigma_z^2} \right) G$$

Composite of three orthogonally oriented lobed patterns

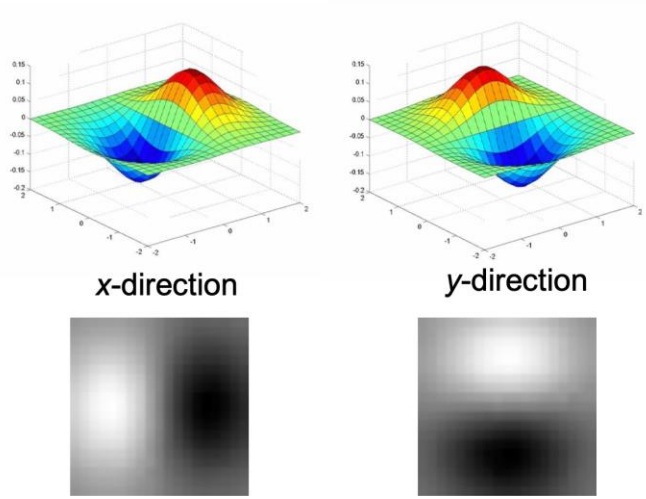

Parameters of the Gaussian derivative functions

- The center of the Gaussian function is randomly selected within an inner mask of the original anthropomorphic phantoms

- The standard deviation of the Gaussian function are randomly selected within realistic ranges of transformation size

  - 7-10.5 pixels for σ_x and σ_y (pixel size 1 mm)
  - 2.5-3.5 pixels for σ_z (pixel size 3 mm)

- The amplitude of the Gaussian derivatives α_x, α_y, α_z are randomly scaled according to realistic ranges of transformation amplitude

  - 3-7.5 pixels for α_x and α_y (pixel size 1 mm)
  - 1-2.5 pixels for α_z (pixel size 3 mm)

- For each central slice, three adjacent slices are included on either side, resulting in an input slab of seven consecutive slices

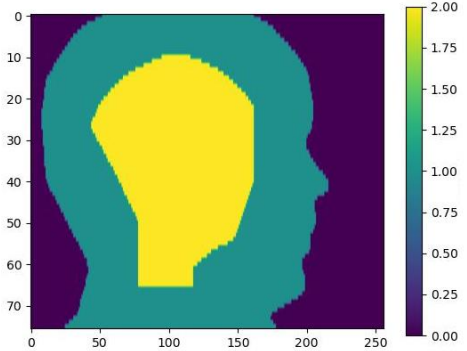

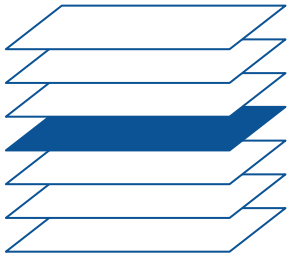

Dataset

- 10 anthropomorphic phantoms, 3 transformations applied to each phantom, 5 samplings per transformation
  - 60 slabs selected for the “full training” study, 50 for training, 10 for validation
  - 10 additional slabs used for testing, sourced from phantoms excluded from training and validation
- Deterministic “subset training” studies with batch sizes equal to the training data size (1, 2, 4, and 8 slabs) and 1 validation slab (i.e., the “example slab”)
- Loss Function based on mean squared error (MSE), computed with respect to the ground truth image
- Task-specific evaluation metrics calculated within the region of applied transformation, defined by a threshold on the magnitude of the ground truth transformation field
  - Root mean square error (RMSE)
  - Structural similarity index (SSIM)

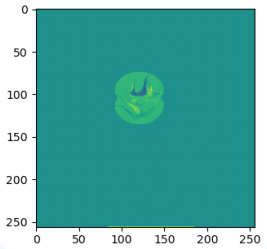

“Subset training” batch size

- Based on deterministic “subset training”, the batch size (BS) is set to 4
  - BS 1: Overfitting (model capacity > size of the training data), inaccurate gradient (relative to the full-dataset gradient) but deterministic
  - BS 2: Overfitting, improved generalization gap, more accurate but unstable gradient
  - BS 4, 8: Overfitting, stable generalization gap

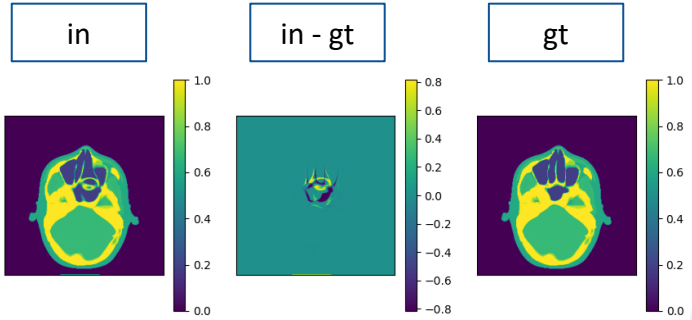

@minimum validation MSE

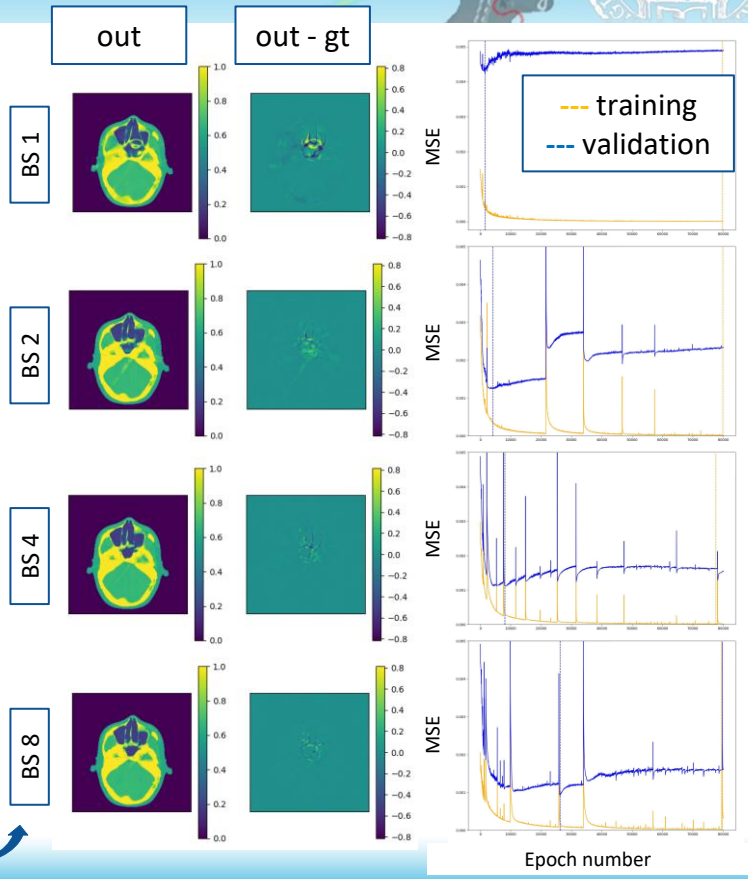

“Subset training” learning rate

- The learning rate for the LPD network is reduced (from 5×10^{-4} to 5×10^{-5}) to achieve more stable training

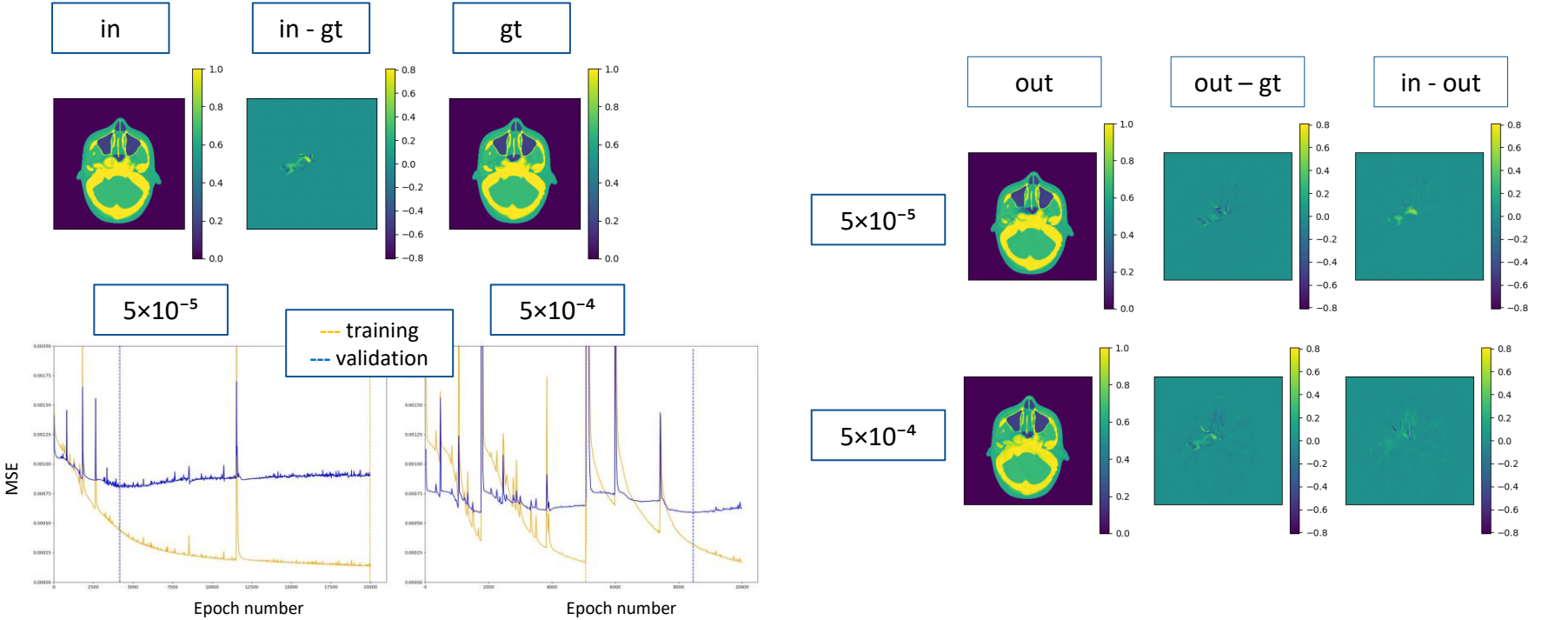

“Subset training” learning rate

- The learning rate of the U-LPD network is increased (from 5×10^{-5} to 5×10^{-4}) to achieve better training

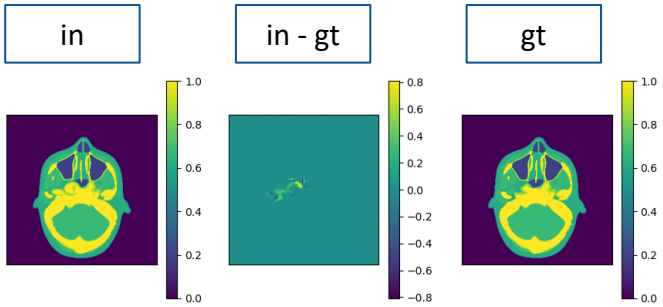

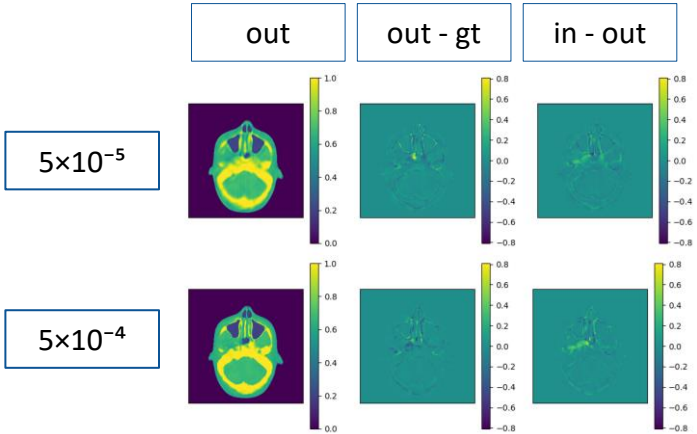

- Gradients propagate through both the LPD blocks and the U-Net, and a higher learning rate counteracts gradient attenuation caused by the increased network depth and normalization layers

- The training and validation curves of the U-LPD network exhibit high stability and low sensitivity to variations in the learning rate, with signs of overfitting observed for values greater than 1×10^{-3}

“Subset training” stopping criterion

- The LPD and U-LPD are trained using different learning rates, since the stopping criterion is generally independent of the learning rate
  - Window size of 600 epochs, tolerance of 1%, patience of 800 epochs

@”example slab”

	LR	RMSE	SSIM
LPD	5×10^{-5}	2.46×10^{-2}	0.870
	5×10^{-4}	2.60×10^{-2}	0.854
U-LPD	5×10^{-5}	2.68×10^{-2}	0.829
	5×10^{-4}	2.91×10^{-2}	0.804

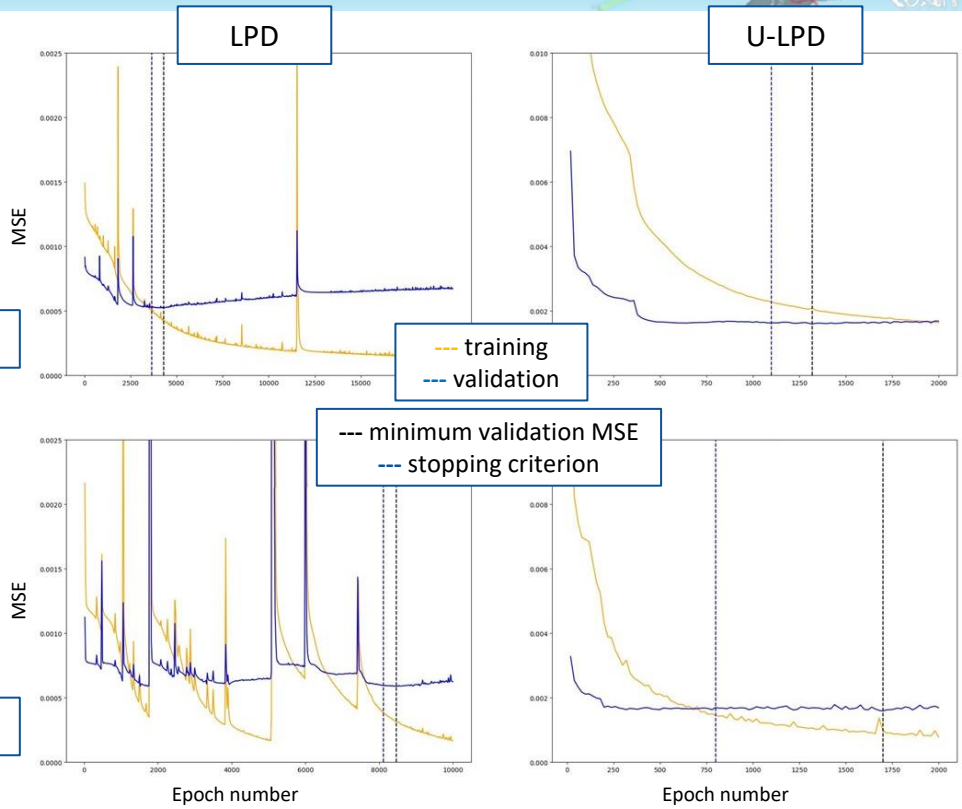

“Full training”
LPD

- The LPD is trained in “full training”

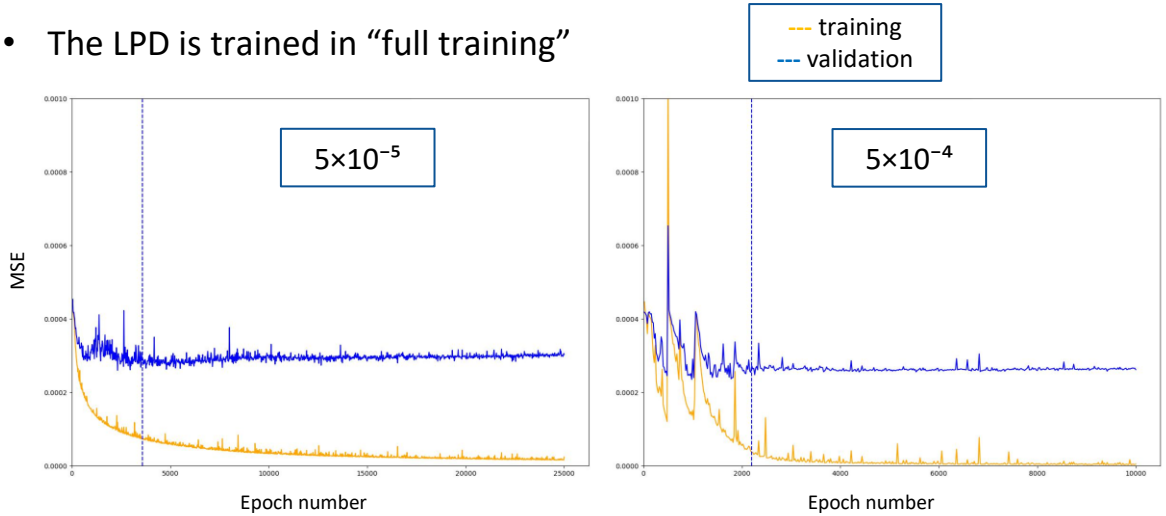

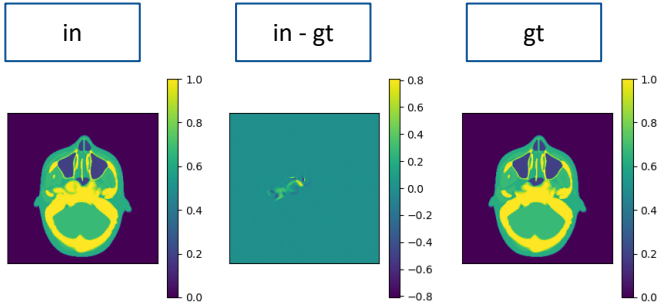

@stopping criterium

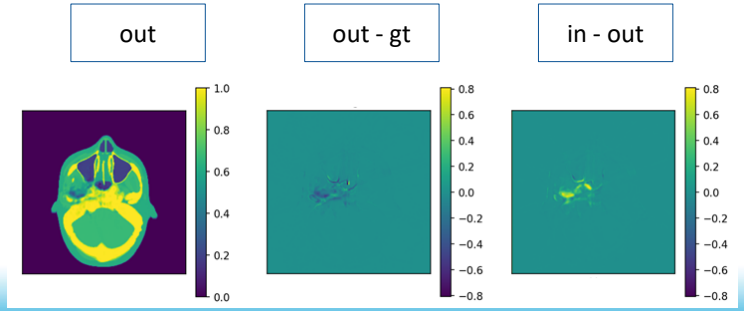

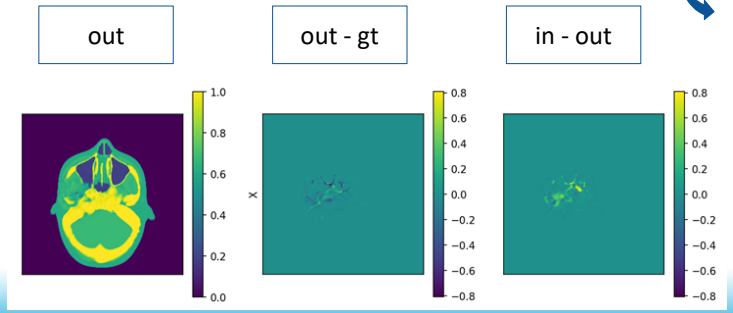

“Full training”
U-LPD

- The U-LPD is trained in “full training”

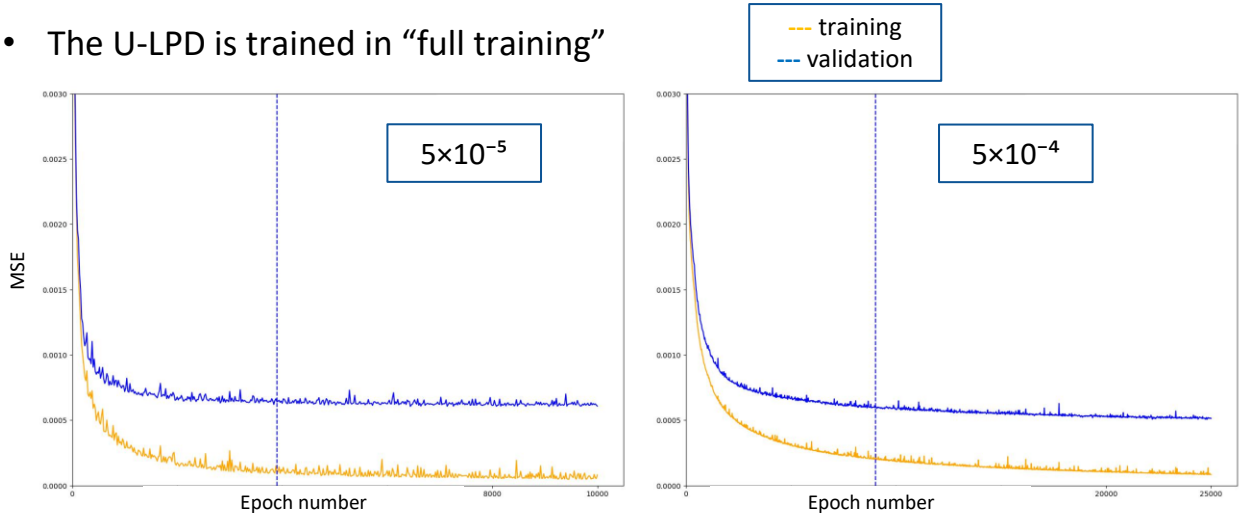

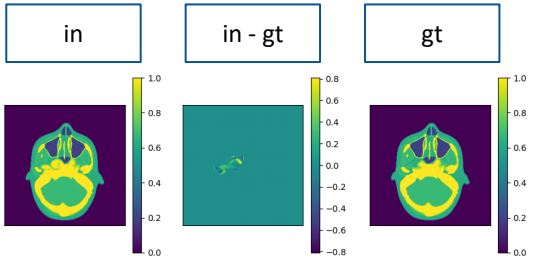

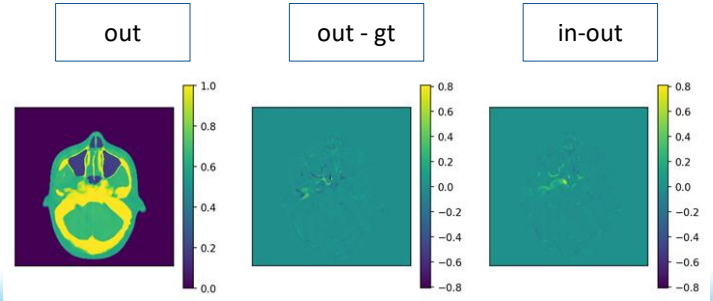

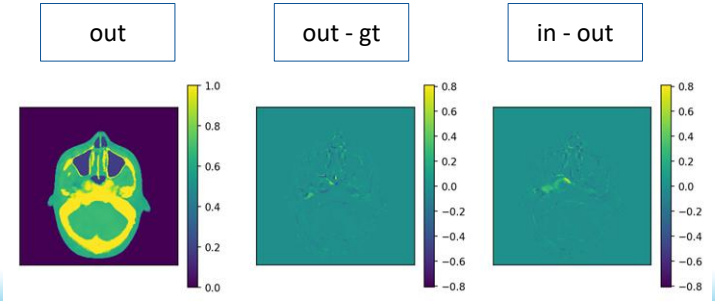

@stopping criterium

Task-specific evaluation metrics validation dataset

- The metrics suggest that both the LPD and U-LPD networks are capable of capturing the transformation
- The U-LPD network performs comparably to the LPD network while demonstrating more stable training and validation curves

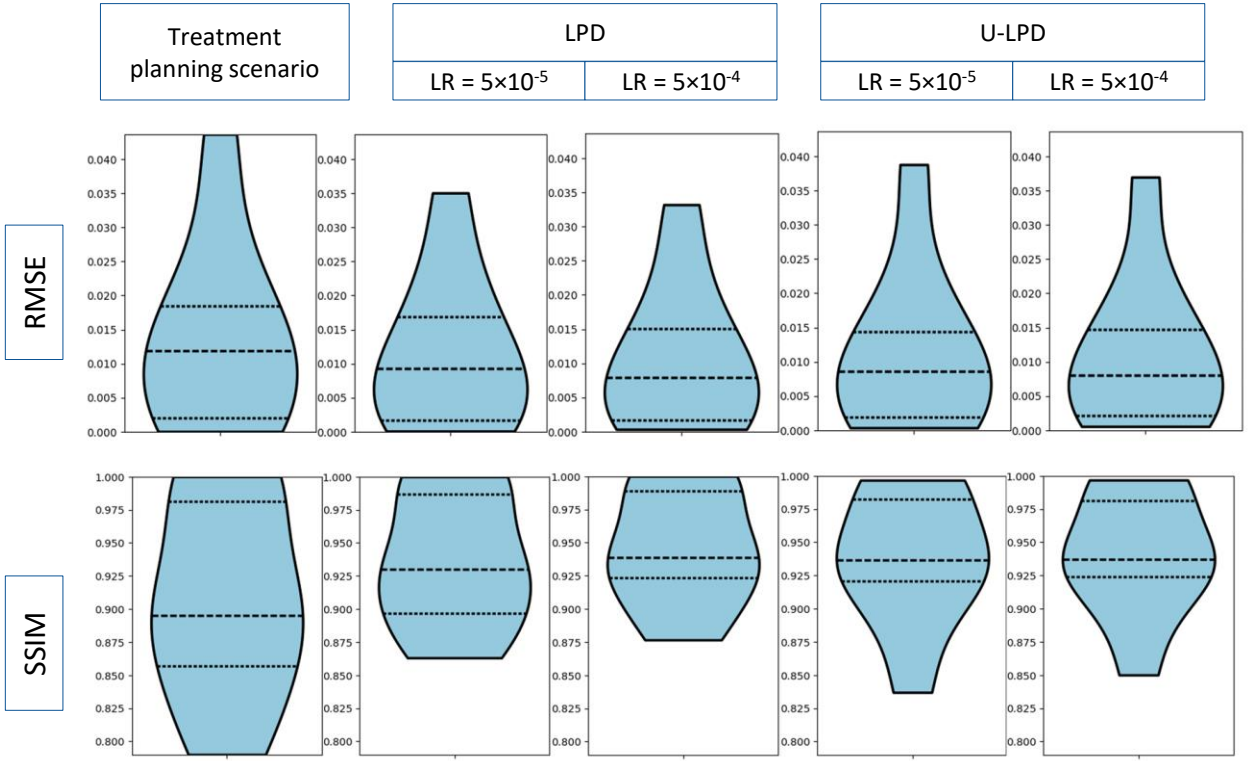

Task-specific evaluation metrics test dataset

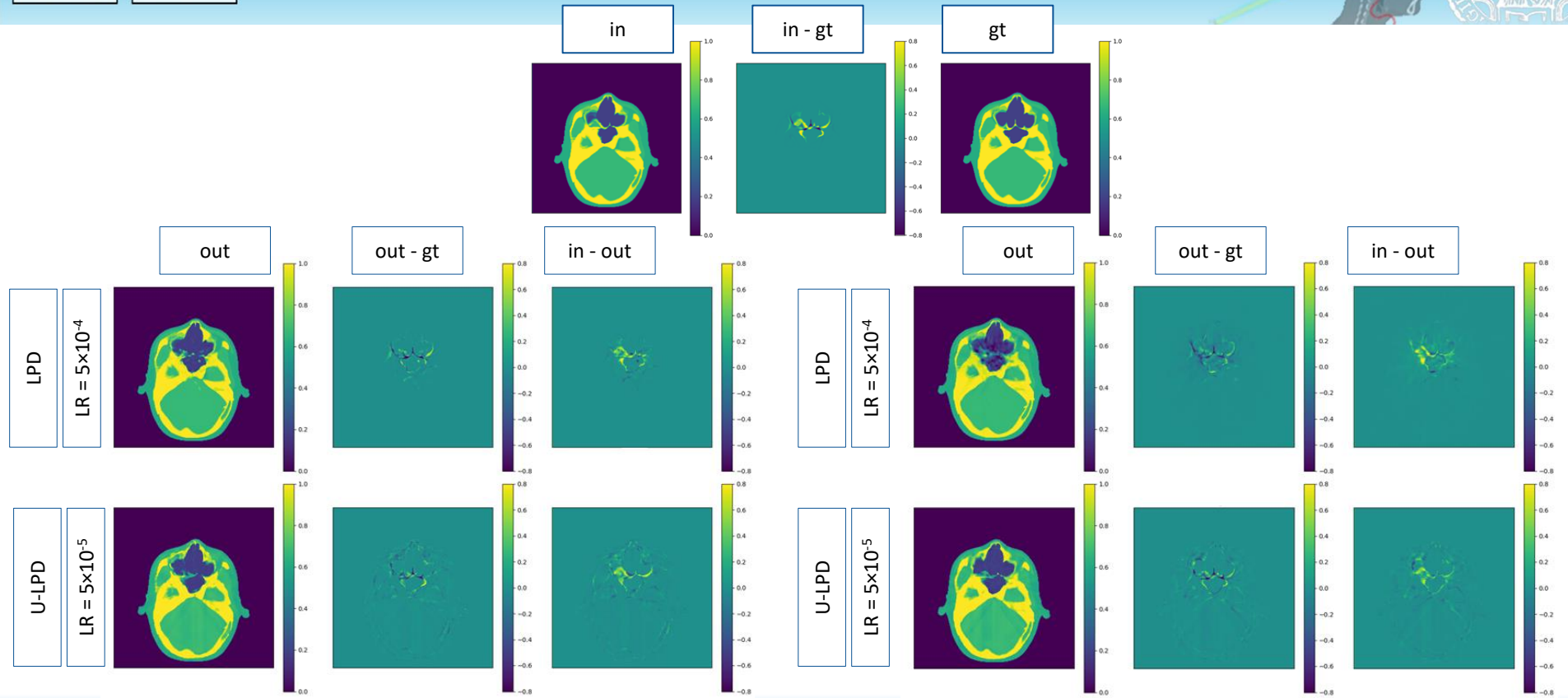

LMU LUDWIG-MAXIMILIANS-UNIVERSITÄT MÜNCHEN

Task-specific evaluation metrics test dataset

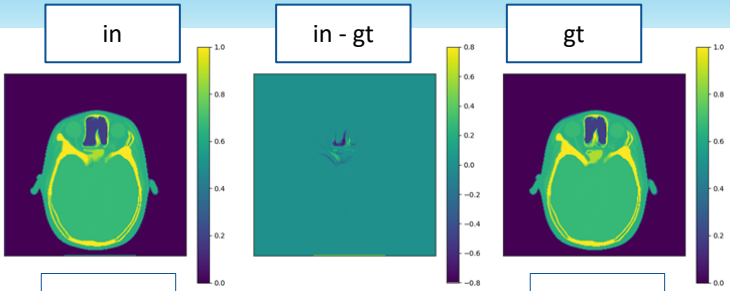

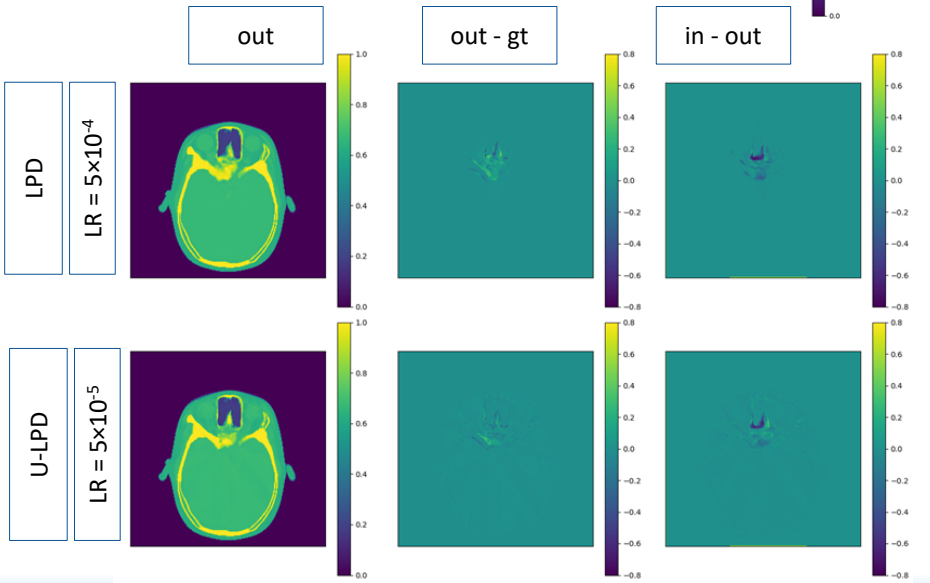

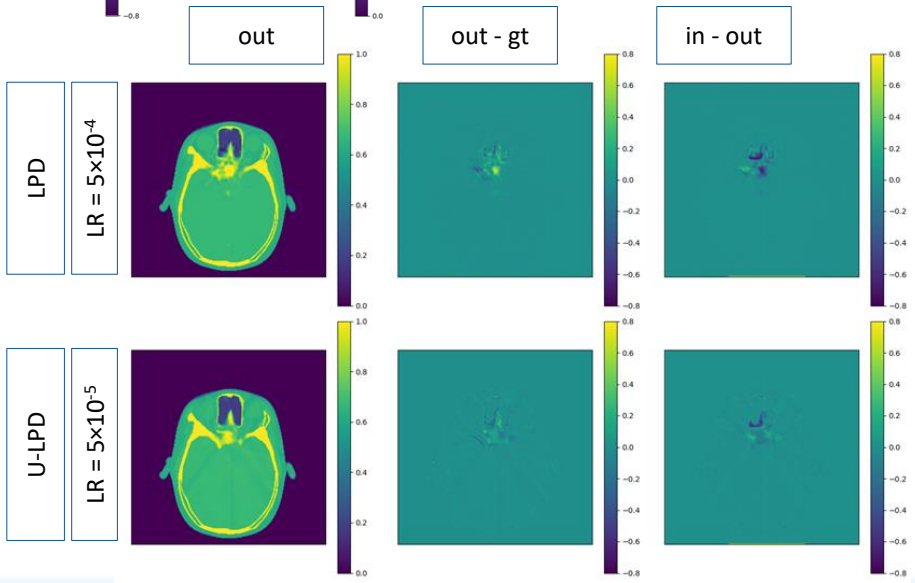

Task-specific evaluation metrics test dataset

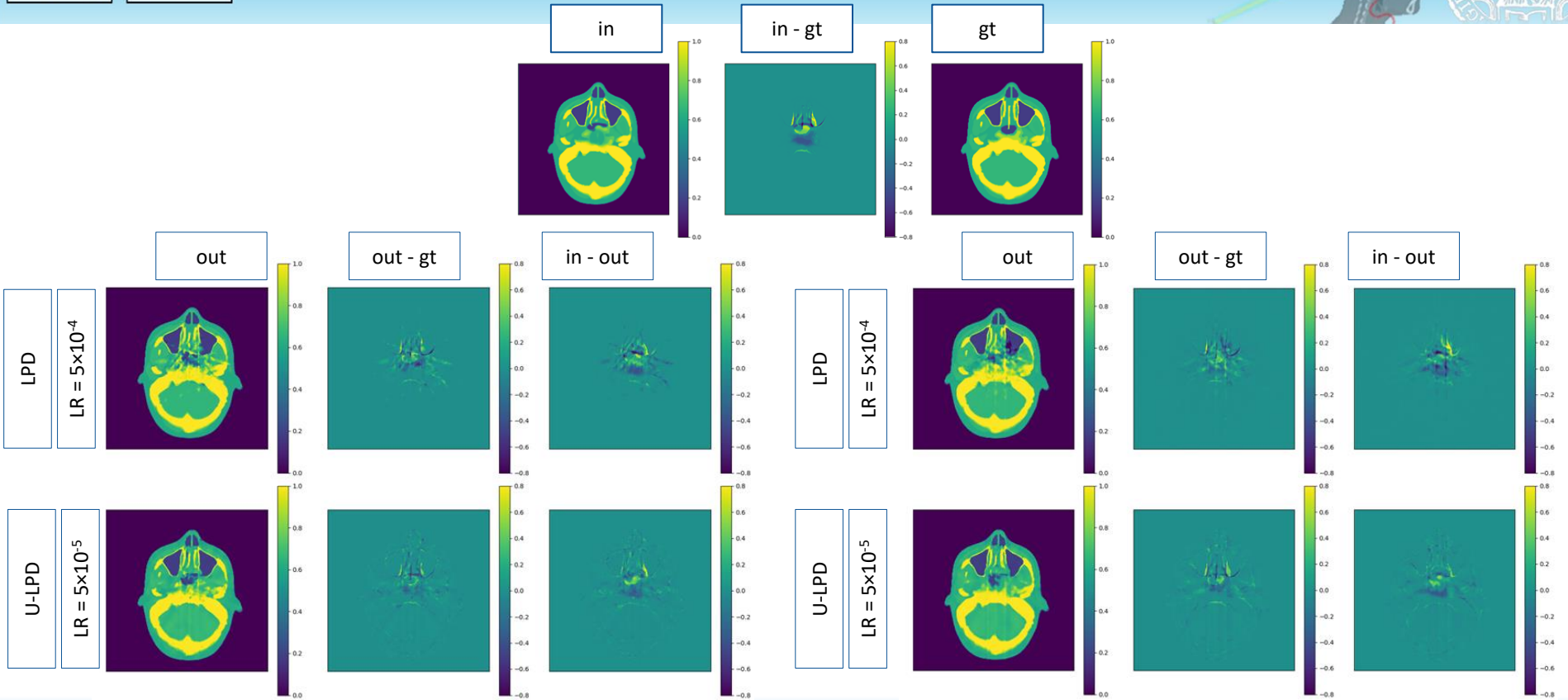

Task-specific evaluation metrics test dataset

- The deformations applied to the phantom in the test dataset result in greater intensity differences relative to the ground truth, and this is reflected in the evaluation metrics
- The metrics confirm the results observed on the validation dataset, highlighting both the ability of the two architectures to capture the deformation

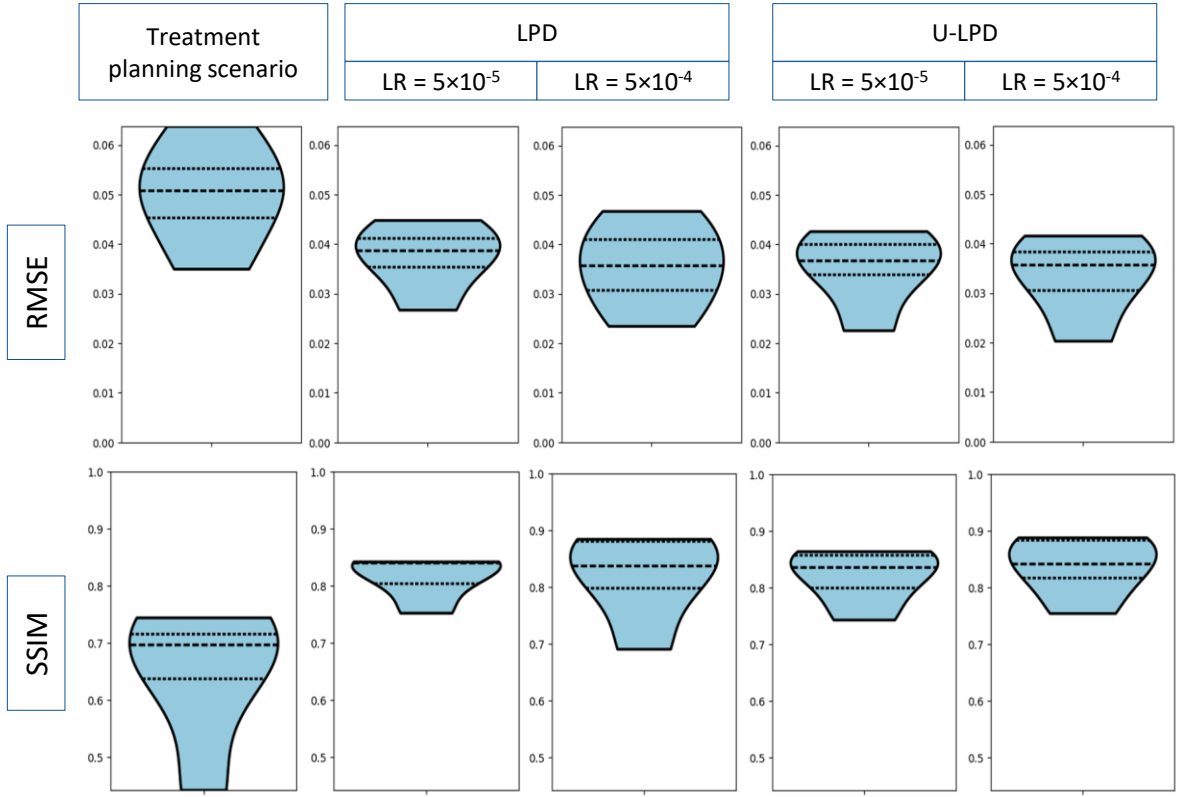

Treatment adaptation based on sparse ion radiographies

- Further investigation of the architecture → Explore optimal placement and depth of U-Nets
  - Early U-Nets: may capture features on coarse reconstruction
  - Late U-Nets: may overcomplicate an already refined reconstruction

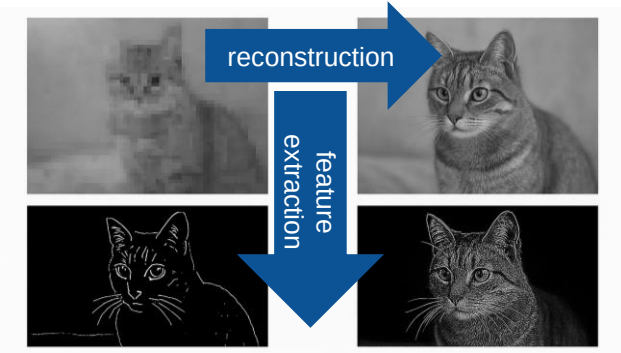

- Combination with the calibration inaccuracies → Explore joint inference of “image and motion”

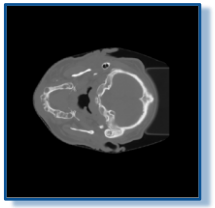

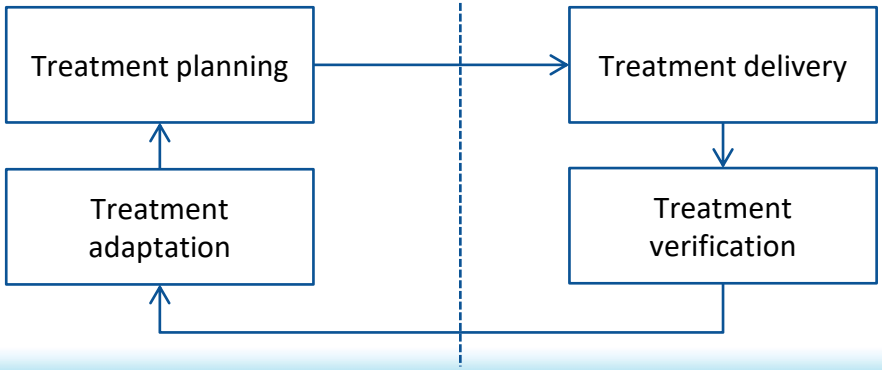

Treatment adaptation based on sparse ion radiographies

- Monte Carlo simulations on patient data → Explore patient-specific and detector-specific realistic data

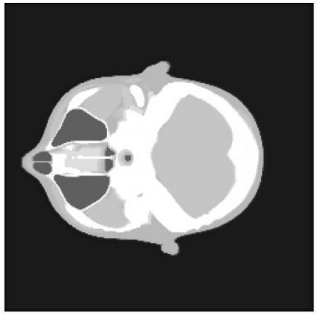

phantom data

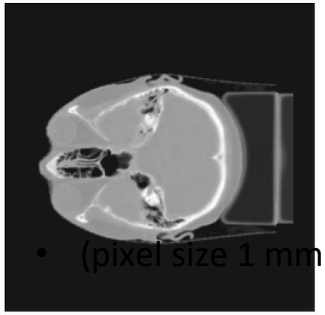

- (pixel size 1 mm)

clinical data

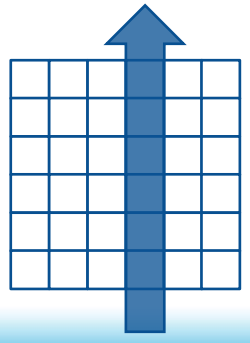

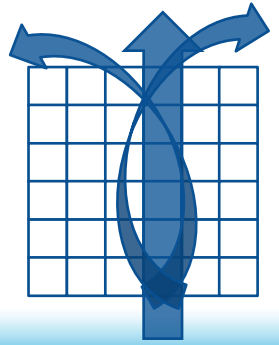

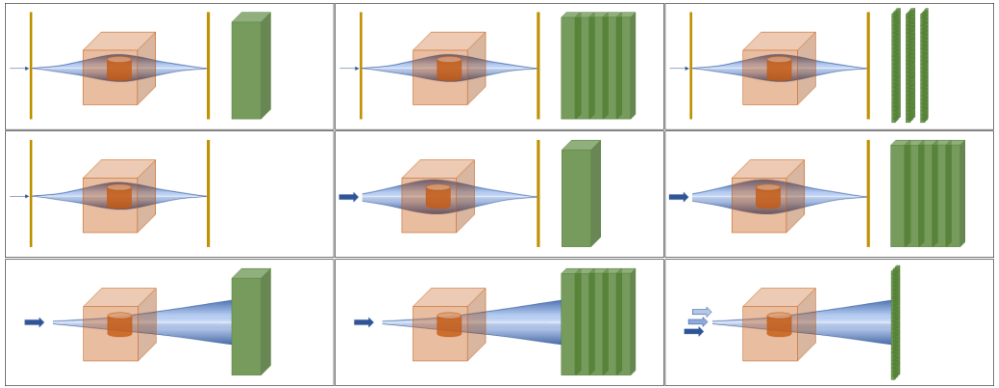

Paganelli, C., Gianoli, C., & Knopf, A. (2024). Imaging in Particle Therapy: Current practice and future trends. IOP Publishing.

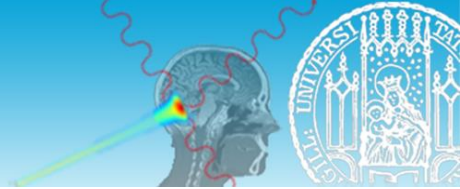

Thank you for your attention

Additional slides

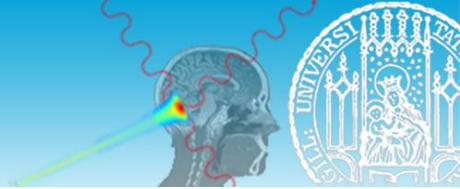

The role of ion imaging in treatment planning

- The optimization of the X-ray CT image calibration using sparse ion radiographies simplifies the tomographic image reconstruction problem, with the aim of reducing calibration inaccuracies
  - The prior information of the calibrated X-ray CT image and the reduced number of unknowns (i.e., the points of the calibration curve) are hypothesized to serve the solution of the ill-posed inverse problem

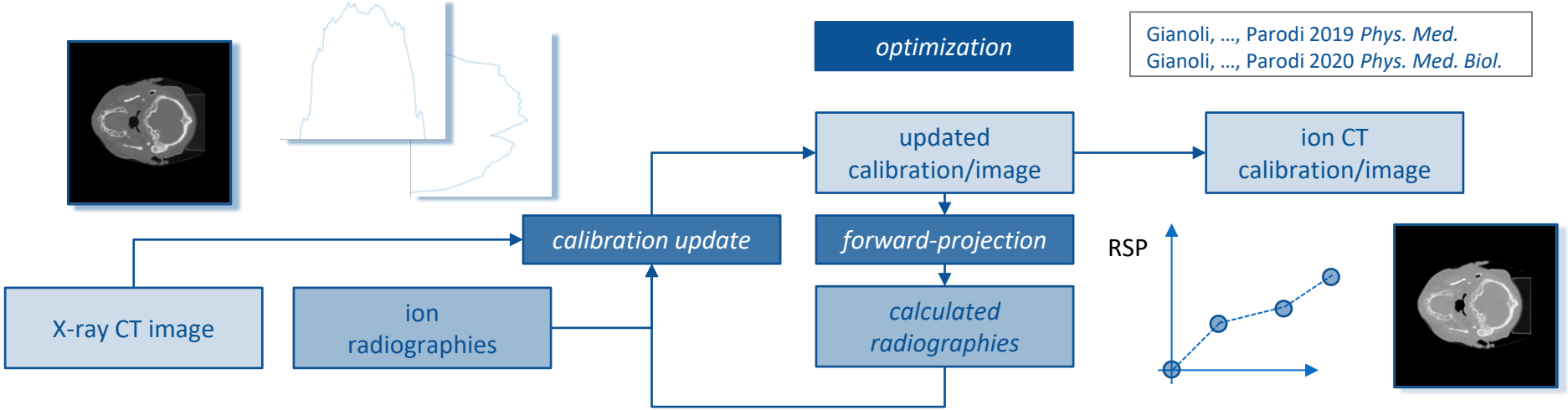

The role of ion imaging in treatment adaptation

- A formulation of the image registration problem based on sparse ion radiographies has been firstly proposed, aiming to minimize anatomical changes in adaptive radiation therapy
  - The forward-projection operator is exploited to transform the X-ray CT image according to the sparse ion radiographies

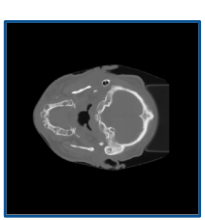

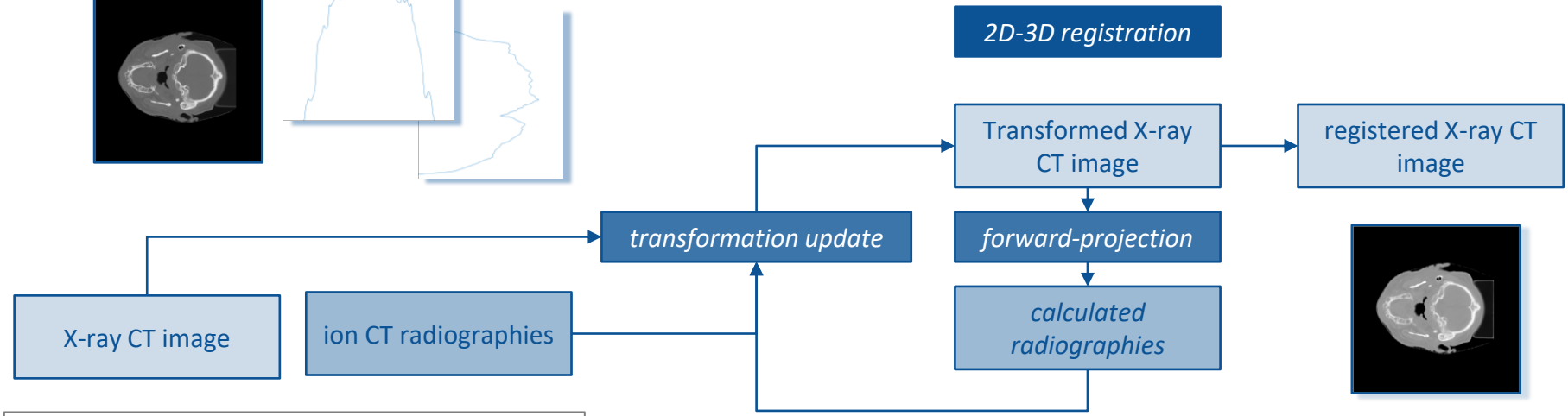

Palaniappan, …, Parodi, Gianoli 2021 *Phys. Med. Biol.*
Palaniappan, …, Parodi, Gianoli 2022 *Phys. Med. Biol.*

“Subset training” learning rate

- LPD: The learning rate is reduced (from 1×10^{-4} to 5×10^{-5}) to achieve more stable training

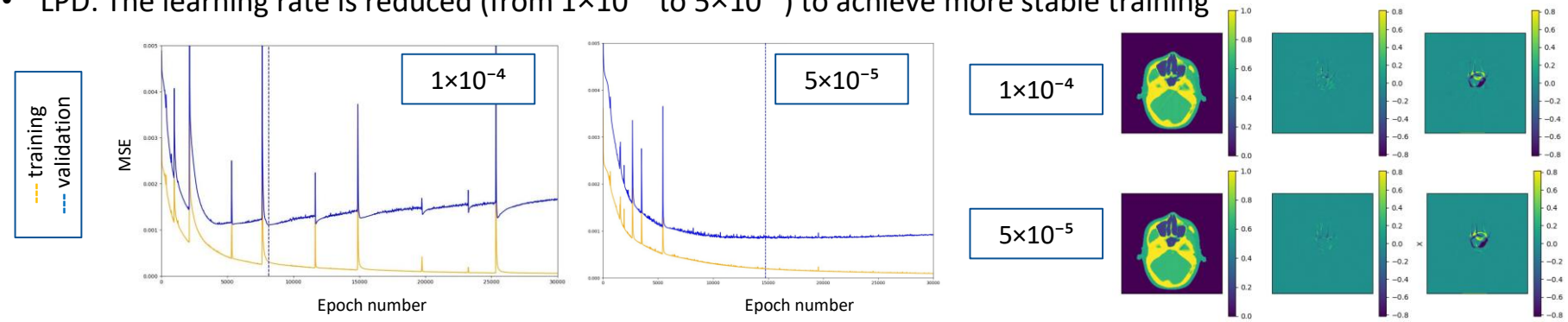

- U-LPD: The learning rate is increased (from 5×10^{-5} to 5×10^{-4}) to achieve more stable training